NJC

ROYAL SOCIETY OF CHEMISTRY

PAPER

View Article Online
View Journal | View Issue

Cite this: *New J. Chem.*, 2023, **47**, 9186

Graphene oxide promotes aggregation-induced emission in binary solvent mixtures†

Souvik Pandit, Sanyukta Bhattacharjee and Debabrata Seth *

The role of graphene oxide (GO) in quenching the emission properties of various organic fluorophores is well known. However, promoting prototropism of various organic fluorophores or inducing fluorescence enhancement is less documented in the literature. The role of GO on the emission properties of fluorophores in binary-solvent mixtures is not very well studied. In this article, we report the photophysical behavior of fluorescein (NaFlu) molecules in the presence as well as in the absence of GO, in neat solvents and water–polar aprotic solvent binary mixtures. In the presence of GO, addition of polar aprotic solvents promotes solvent-induced aggregation of NaFlu in water, *i.e.* aggregation-induced emission (AIE), since due to the aggregate formation there is a restriction in the intramolecular rotation of NaFlu molecules, and the chances of non-radiative relaxation pathways decreases. In the absence of GO, NaFlu forms aggregates which leads to π–π coplanar interactions between NaFlu molecules leading to excimer species formation that prefers to decay through non-radiative pathways thus promoting an aggregation-caused quenching (ACQ) phenomenon. Therefore, the presence of GO facilitates the AIE of NaFlu molecules in different binary solvent mixtures. This property of GO will be helpful to create novel GO nanocomposites for device and biosensor applications.

Received 1st March 2023,
Accepted 4th April 2023

DOI: 10.1039/d3nj00995e

rsc.li/njc

1. Introduction

Fluorescein is known to exist in seven different prototropic forms as shown in Scheme 1: four charged forms and three neutral forms each exhibiting distinguishable photophysical properties.[1] High photo-stability and a high quantum yield are some of the many unique spectroscopic properties that fluorescein exhibits. This is due to the presence of a rigid and large pi-conjugated structure that fluorescein possesses.[2] Fluorescein is widely used as a standard molecule for calculating the quantum yield,[3] and it exhibits a wide array of applications known to mankind.[4–13]

One of the notable members of the graphene family is graphene oxide (GO).[14] GO is known to form stable colloidal suspensions.[15] Scheme 2 showcases the various functional groups on the surface of GO. GO has drawn the attention of the scientific community owing to its unique set of properties[16–18] and due to its diverse applications.[19–26]

Binary mixtures involving non-aqueous and aqueous solvents are very interesting systems owing to the non-ideal properties and anomalous behavior of binary mixtures. Substances which are less soluble in neat solvents are readily soluble in binary mixtures.[27] To comprehend the diverse set of properties of binary mixtures, one must know the composition of the involved components.[28] In most cases it has been seen that binary solvents function as an inhomogeneous mixture and are non-ideal to both dynamical properties such as cluster diffusion, solvation energy, *etc.* and static properties such as refractive index, viscosity, *etc.*[28–33]

A few studies are reported in the literature regarding the photophysical changes of a few organic fluorophores induced by GO. GO is known for enhancing the fluorescence of a hydrophilic molecule 7-(diethylamino)-coumarin-3-carboxylic acid (7-DCA). GO acts both as an enhancer and a quencher of fluorescence of 7-DCA depending upon the solvent choice.[34] GO also promotes prototropism of lumichrome,[35] Nile blue A (NB)[36] and the oxazine-170 perchlorate (OXO) molecule.[37] GO induces hydrogen abstraction as well as hydrogen elimination as a result of which prototropism occurs.[36,37] This is mainly due to the presence of various oxygen functional groups on the GO surface. Therefore, to further understand the role of GO, we have chosen the fluorescein (NaFlu) molecule to comprehend its photophysical changes in binary solvent mixtures (water–polar aprotic solvents). The solvatochromism of NaFlu in aqueous aprotic solvents is reported in the literature, where the authors have reported that hydrogen bonding causes hypsochromic shift whereas polarity leads to bathochromic shift.[2] The solvatochromic properties of the NaFlu dye in a water–alcohol mixture are

Department of Chemistry, Indian Institute of Technology Patna, Patna 801103, Bihar, India. E-mail: debabrata@iitp.ac.in; Tel: +91-6115-233028

† Electronic supplementary information (ESI) available: Absorption, emission, time-resolved emission, Raman spectra, FE-SEM, and FLIM images. See DOI: https://doi.org/10.1039/d3nj00995e

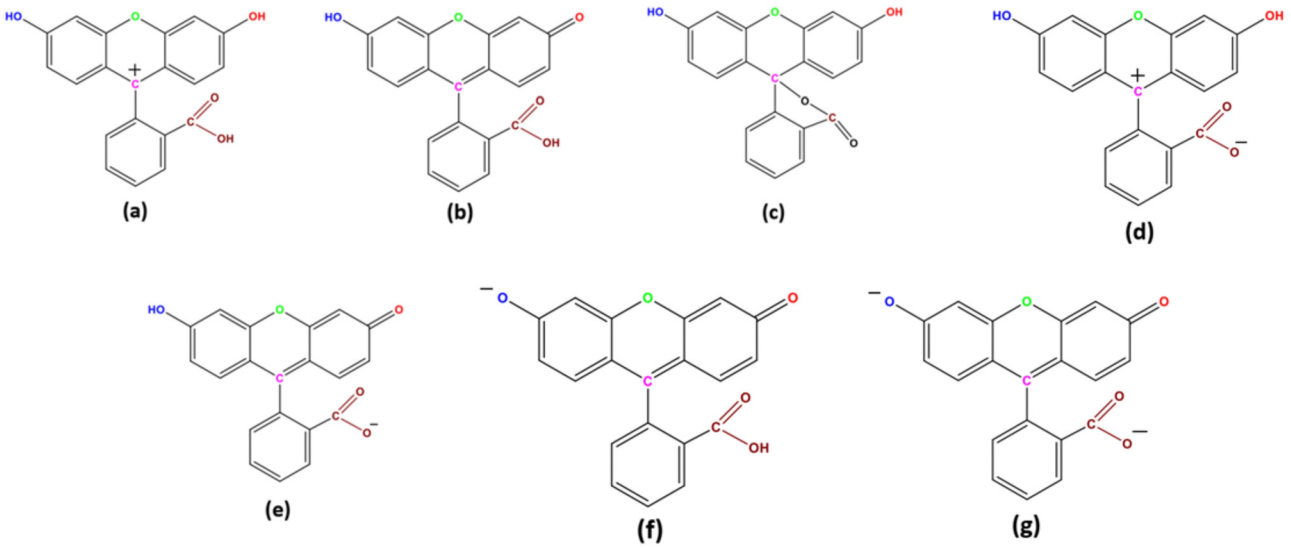

Scheme 1 Various forms of fluorescein: (a) cation, (b–d) neutral, (e and f) anion, and (g) dianion.

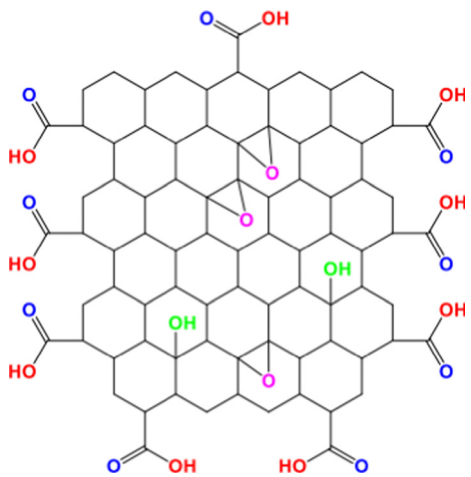

Scheme 2 Various functional groups present in GO.

documented in the literature which states that the spectral shift NaFlu undergoes is influenced by polarity as well as hydrogen bonding acidity of the medium under investigation.[38,39] In this work we found another interesting property of GO, promoting aggregation-induced emission (AIE) of NaFlu in binary solvent mixtures. π–π coplanar interactions between NaFlu molecules lead to excimer species formation that prefers to decay through non-radiative pathways thus promoting an aggregation-caused quenching (ACQ) phenomenon. Therefore, the presence of GO facilitates the AIE of NaFlu molecules in different binary solvent mixtures.

2. Materials and methods

2.1 Materials

Sodium fluorescein (NaFlu) was bought from Sigma-Aldrich and used without further purification. From Sigma-Aldrich, GO was purchased and used as received. The various solvents used in this project were acetonitrile (ACN), *N*,*N*-dimethyl formamide (DMF), dimethyl sulphoxide (DMSO), tetrahydrofuran (THF) and triple distilled water.

2.2 Sample preparation

In 4 mL of each solvent, 2 mg of GO was dissolved, *i.e.* 0.5 mg mL^{-1} is the concentration of GO prepared. All the prepared GO dispersions were sonicated in a cold water bath for 1 h. This was performed to dispense the heat generated during the ultrasonication process. The concentration of NaFlu throughout all the experiments was 1×10^{-5} M.

2.3 Instrumentation

2.3.1 Steady-state measurements. To collect the absorption and emission as well as excitation data, a Shimadzu UV-Vis spectrophotometer (model number: UV-2550) and a Horiba Jobin Yvon spectrofluorometer (model number: Fluoromax 4) were used, respectively. For obtaining the data, a quartz cuvette was used. For all the experiments, the temperature was maintained at 298 K using a Peltier controlled cuvette holder for the fluorescence study and for the absorbance study, a Jeiotech refrigerated bath circulator was used.

The actual spectral changes of NaFlu in the presence of GO were corrected using the inner filter effect which is shown in eqn (1).

$$F_{obs} = F_{corr} \times 10^{-\left(\frac{A_{ex}d_{ex}}{2}\right)-\left(\frac{A_{em}d_{em}}{2}\right)} \quad (1)$$

F_{corr} symbolizes the fluorescence intensity after eliminating the inner filter effect, and F_{obs} denotes the fluorescence intensity observed. d_{ex} and d_{em} denote the path length (cm) of the cuvette for excitation and emission respectively. A_{ex} and A_{em} symbolize the absorbance intensity values for the excitation and emission wavelengths respectively.

2.3.2 Fluorescence lifetime measurements. The fluorescence dynamics of NaFlu molecules in different environments was analysed using the picosecond time-correlated single-photon counting (TCSPC) technique. A time-resolved fluorescence spectrophotometer from Edinburgh Instruments (model: Life Spec-II, U.K.) was used for this purpose using a picosecond diode laser with an excitation wavelength of 405 nm exciting the NaFlu molecule. At the magic angle (54.7°), a Hamamatsu MCP PMT (3809U) detector was used to obtain the fluorescence transients. The temperature was held constant at 298 K with the help of a Peltier-controlled cuvette holder from Quantum North-West (Model: TLC-50). To analyse and fit the decays obtained F-900 decay software was used. The χ^2 parameter value determined the goodness of the fitting.

3. Results and discussion

3.1 Steady-state absorption and fluorescence measurements

3.1.1 Studies on the interaction of NaFlu with GO in water. For absorption measurements, we have performed the baseline correction with respect to the dispersion solution of GO in the respective solvent in each experiment, so that any contribution from the latter is eliminated. In neat water, as shown in Fig. 1, absorption spectra showcase the presence of the dianionic form of NaFlu at 487 nm which corresponds to Scheme 1(g) followed by the contribution of the monoanionic form of the dye (shoulder) at 460 nm which corresponds to Scheme 1(f).[40] Sjoback *et al.*[41] very lucidly highlighted the different protonated forms of NaFlu along with their corresponding absorption spectra. On addition of 3 and 15 μg mL^{-1} of GO, both the monoanionic and dianionic forms of NaFlu are present in water followed by a decrement in absorption intensity. However, for 35 μg mL^{-1} GO, the peak at 487 nm experiences a blue shift by 12 nm, *i.e.* a new peak is formed at 475 nm. The peak at 460 nm experiences a blue shift by 8 nm and a new peak is formed at 452 nm. On addition of 90 μg mL^{-1} GO, the peak at 452 nm is prominent which corresponds to the monoanionic form of the dye.[41] The interesting aspect regarding this observation is that the dianionic form of NaFlu, for an initial concentration of 15 μg mL^{-1} GO, is present in water; however, for 35 μg mL^{-1} and beyond that concentration of GO only the monoanionic form tends to exist in the solution. Hence, GO not only decreases the amplitude of the 486 nm component of NaFlu, but also promotes the conversion of the dianionic form of NaFlu to the monoanionic form. Therefore, the absorption spectrum reveals that NaF attaches on the GO surface and the monoanionic form of NaFlu is predominant. From the absorption data, we thus

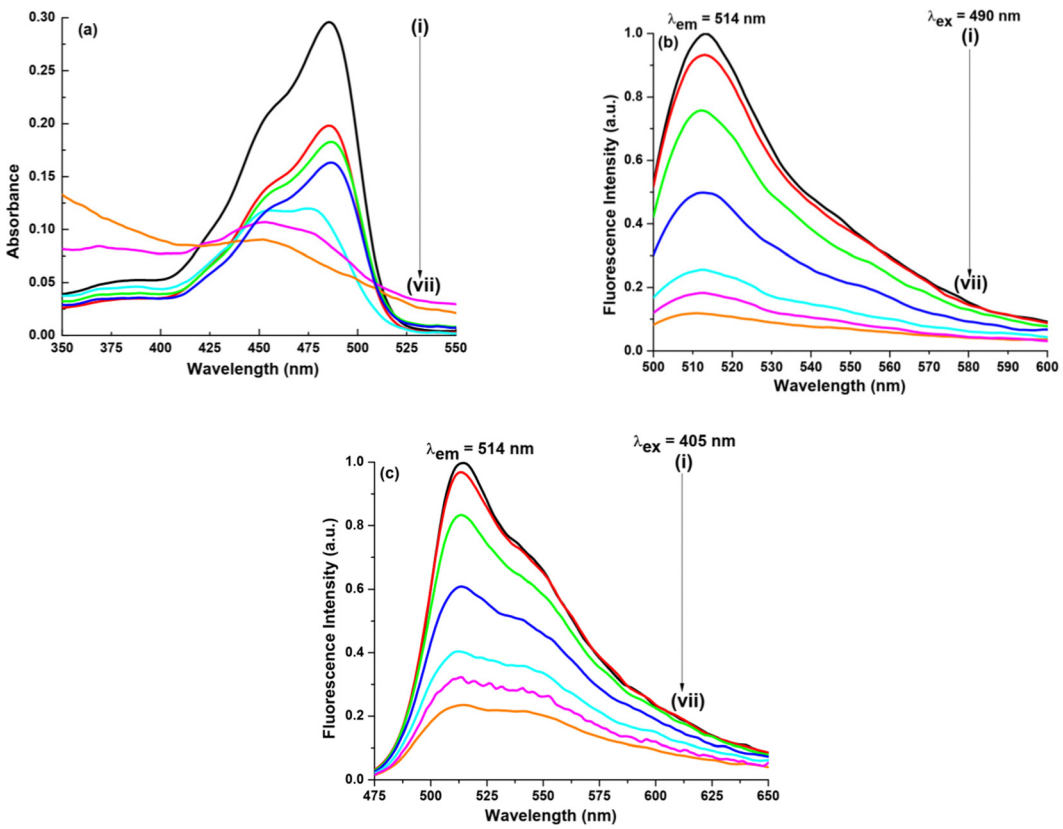

Fig. 1 (a) Absorption spectral profile of NaFlu with GO in water: (i) NaFlu, (ii) NaFlu + 3 mg mL^{-1} GO, (iii) NaFlu + 15 mg mL^{-1} GO, (iv) NaFlu + 25 mg mL^{-1} GO, (v) NaFlu + 35 mg mL^{-1} GO, (vi) NaF + 60 mg mL^{-1} GO and (vii) NaFlu + 90 mg mL^{-1} GO. Fluorescence emission spectra of NaFlu with GO in water (b) λ_{ex} = 490 nm and (c) λ_{ex} = 405 nm: (i) NaFlu, (ii) NaFlu + 3 mg mL^{-1} GO, (iii) NaFlu + 15 mg mL^{-1} GO, (iv) NaFlu + 25 mg mL^{-1} GO, (v) NaFlu + 35 mg mL^{-1} GO, (vi) NaFlu + 60 mg mL^{-1} GO and (vii) NaFlu + 90 mg mL^{-1} GO.

decided to undertake emission studies at two excitation wavelengths, which are 490 nm and 405 nm. We chose 490 nm to excite the dianionic form of NaFlu, whereas 405 nm was used to excite any other lower absorbing forms of NaFlu as well since we used a 405 nm laser to collect time-resolved emission decays. Upon excitation at 490 nm, it is observed that the emission peak is generated at 514 nm which agrees well with the reported data in the literature.[42] This characteristic peak at 514 nm undergoes a prominent reduction with respect to its intensity upon the addition of 3 μg mL^{-1} GO. This trend is followed with the gradual addition of GO up to 90 μg mL^{-1} without any change in the emission position. In short, GO basically acts as a quencher. The same behaviour is obtained when excited at 405 nm as shown in the ESI.† Now let's decipher why GO behaves as a quencher? The presence of various oxygen functional groups and the existence of 2D sp^2 carbon atoms in a single layer impart GO with many unique properties such as stability in a water medium,[43] amphiphilicity,[44] surface modifications[45] and adsorption of molecules on the GO surface *via* hydrogen bonding[46] and pi–pi stacking.[47] Thus when GO is added gradually to water having NaFlu molecules, the latter undergoes adsorption on the GO surface, followed by quenching of fluorescence intensity. Another possible reason for such behaviour is that the pi electrons of NaFlu can interact with the pi electrons of GO sheets *via* a non-covalent interaction as a result of which the fluorescence signal of NaFlu decreases.[48–50] A few studies in the literature have suggested that the intensity of NaFlu quenches due to the formation of a non-emissive supramolecular moiety in the presence of graphene.[51,52] So the presence of NaFlu within GO which acts as a host might be another possible reason for the prominent quenching of both the absorption and fluorescence signal. In water, the absolute quantum yield value (ABQY) of NaFlu is 0.92 which agrees with the literature value.[3] On addition of 35 μg mL^{-1} of GO, the ABQY value decreases to 0.34 as shown in Table S1 (ESI†) which supports the fact that GO acts as a quencher. The absorption and fluorescence studies regarding NaFlu in the presence of GO in ACN, DMSO, DMF and THF are explained in a detailed manner in Fig. S1 (ESI†). In the case of water, we have seen the conversion of various forms of NaFlu, which draws our attention. So for the next upcoming sections, we have considered NaFlu-GO in the water system and tried to monitor the photophysical changes that NaFlu undergoes on addition of various polar aprotic solvents, *i.e.* binary mixtures both in the presence and in the absence of GO.

3.1.2 Fluorescence quenching of NaFlu with GO in water. The Stern–Volmer equation determines the nature of binding between a fluorophore and a quencher where K_{SV} denotes the Stern–Volmer constant of the complex formed. The plot of I_0/I *vs.* [Q] should be a straight line where K_{SV} denotes the slope.[53] Nonetheless sometimes upward curvature, *i.e.* positive deviation from linearity, is also observed in systems that involve only one type of quenching, *i.e.* static or dynamic quenching.[54–58] In our case on addition of GO to NaFlu in water, the fluorescence intensity of NaFlu decreases. The almost constant lifetime values as discussed in the lifetime section clearly indicate that static quenching is prominent due to the stable non-fluorescent complexes between GO and the NaFlu molecules formed. However, in the present case, the upward curvature is prominent for a higher concentration of GO. Campbell *et al.*[59] proposed a generalised model for static quenching which assumes the variable population of a quencher and a fluorophore according to a set of equations:

$$[FQ] = K[F][Q] \quad (2)$$

$$[F] = [F_0] - [FQ] \quad (3)$$

$$[Q] = [Q_0] - [FQ] \quad (4)$$

Here $[F_0]$ and $[Q_0]$ denote the fluorophore and quencher concentrations taken initially, [F] and [Q] are the fluorophore and quencher concentrations for any given time which is after a certain concentration of complexes [FQ] is formed and K denotes the association constant. Thus from this model, a

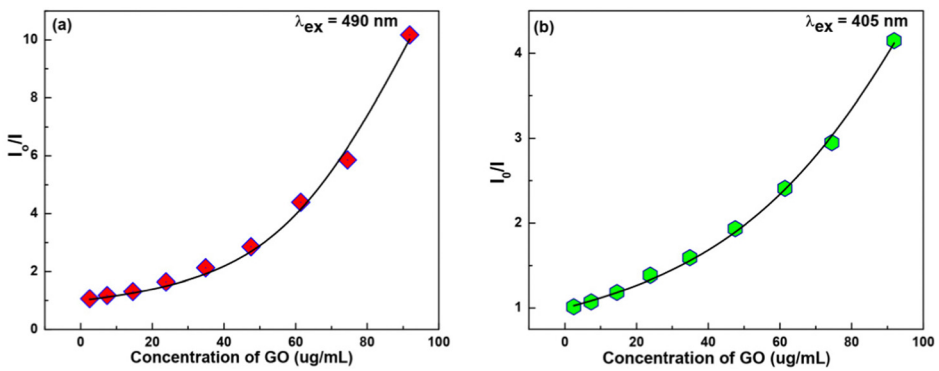

Fig. 2 (a) Stern–Volmer plot for the fluorescence quenching of NaFlu with the addition of GO to water (λ_{ex} = 490 nm) and (b) Stern–Volmer plot for the fluorescence quenching of NaFlu in the presence of GO in water (λ_{ex} = 405 nm).

non-linear equation (eqn (5)) is obtained which is

$$\frac{I_0}{I} = \frac{1}{1-\frac{1}{2F_0}\left[\frac{1}{K_{SV}}+[F_0]+[Q_0]-\sqrt{\left(\frac{1}{K_{SV}}+[F_0]+[Q_0]\right)^2-4[F_0][Q_0]}\right]} \quad (5)$$

Using the above equation, the data are accurately fitted as shown in Fig. 2. We have monitored the quenching of NaFlu in the presence of GO in water at both excitation wavelengths 490 nm and 405 nm, and it is evident that dominant static quenching occurs which is lucidly described by the generalized Stern–Volmer model. The K_{SV} values are $[0.27 \pm 0.02]$ $(\mu g\ mL^{-1})^{-1}$ and 0.11 ± 0.01 $(\mu g\ mL^{-1})^{-1}$ for the excitation wavelengths 490 nm and 405 nm respectively, shown in Fig. 2.

3.1.3 Adsorption phenomenon of NaFlu on the GO surface in different neat solvents. At 298 K, the adsorption isotherms of NaFlu on the GO surface in neat water, ACN and DMSO were determined. The final concentration of GO in respective solvents was fixed with respect to the final concentration of GO used in the fluorescence emission measurements performed. The adsorbed dye (n_s) was obtained using eqn (6)[60]

$$n_s = \frac{(C_o - C_e)V}{m_{ad}} \quad (6)$$

where C_o and C_e denote the initial and equilibrium concentrations of NaFlu respectively, calculated from the fluorescence intensity values of NaFlu at the respective maximum in water, ACN and DMSO. The mass of GO used in the experiment which is the adsorbent is denoted by m_{ad}. V denotes the solution volume. The adsorption isotherm plot of NaFlu on GO is shown in Fig. 3.

Table 1 The parameters of Langmuir isotherms due to the adsorption of NaFlu on GO in various solvents at 298 K

Solvent	n_m (mol g^{-1})	K_L (L mol^{-1})	R^2
ACN	$(4.85 \pm 0.09) \times 10^{-3}$	$(1.40 \pm 0.08) \times 10^{7}$	0.993
DMSO	$(3.71 \pm 0.03) \times 10^{-3}$	$(1.70 \pm 0.04) \times 10^{6}$	0.998
Water	$(2.85 \pm 0.07) \times 10^{-4}$	$(6.60 \pm 0.44) \times 10^{6}$	0.993

Isotherms obtained are then fitted by using the hyperbolic form of the Langmuir model shown in eqn (7):

$$n_s = \frac{n_m . C_{e \cdot K_L}}{1 + K_L \cdot C_e} \quad (7)$$

K_L denotes the equilibrium constant of the adsorption. n_m symbolises the amount of NaFlu adsorbed for full coverage. K_L as well as n_m values are provided in Table 1. The parameters obtained are not comparable with other different solvents because the concentration of GO used is the final concentration of GO for which the fluorescence intensity of NaFlu is prominently quenched. This is because we are concerned only with the adsorption parameters for the final concentration of GO used in different solvents. The adsorption of NaFlu molecules on the GO surface could not be performed in neat DMF and THF solvents. In the case of DMF, the reason for not obtaining the adsorption isotherm is that NaFlu is known for aggregation-caused quenching (ACQ).[61] So while conducting the experiment, on increasing the concentration of NaFlu in the DMF medium, NaFlu showcases the ACQ effect. For THF, the adsorption isotherm could not be extracted simply due to the solubility issue of NaFlu in common organic solvents.[62]

3.1.4 Photophysical studies on the interaction of NaFlu with GO in binary mixtures in the presence and in the absence of GO. In this set of experiments where binary mixtures of solvents are involved we have chosen to fix 35 μg mL^{-1} as the concentration of GO since at this concentration of GO, NaFlu

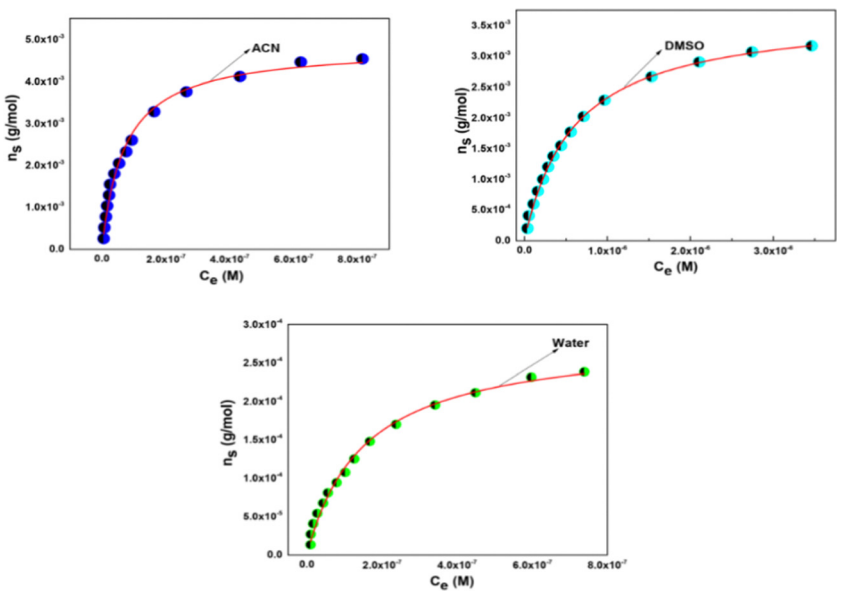

Fig. 3 Adsorption of NaFlu on GO: (a) ACN, (b) DMSO and (c) water.

undergoes a drastic prominent photophysical change as discussed previously. In water, the absorption spectrum of NaFlu includes an intense band corresponding to the dianionic form of NaFlu and a shoulder corresponding to the monoanionic form of the dye. The intense band is due to the allowed π–π* transition occurring on the xanthene moiety, and the shoulder band is due to the *o*-1 transition in symmetric breathing mode.[63] On addition of 35 μg mL^{-1} GO, the dianionic and the monoanionic forms of NaFlu tend to exist. Now we want to monitor how the photophysical properties of NaFlu are modulated in binary mixtures involving ACN, DMF, DMSO and THF.

(a) Water–ACN. ACN is also known to form a few hydrogen bonds with water molecules, eventually thus forming clusters. At $\chi_{ACN} < 0.2$ (where χ means the mole fraction), ACN molecules rupture water structures to a slight extent and water molecules are still self-associated *via* hydrogen bonding. Hence, in our work since $\chi_{ACN} < 0.1$, no rupture of water molecules occurs.[27] In the presence of GO as shown in Fig. 4, on addition of ACN (χ_{ACN} = 0.004), no such change occurs either in the absorption peak position or in the absorption intensity. On addition of ACN (χ_{ACN} = 0.062), however, the intensity amplitude of the 452 nm peak slightly decreases, whereas the intensity amplitude of the 475 nm peak slightly increases. Though the increase or decrease is marginal it is enough to understand that ACN modulates or better to say interacts with NaFlu molecules in the presence of GO in a very subtle manner. In the case of emission spectra, we have used two excitation wavelengths which are 490 nm and 405 nm. The corresponding emission spectra using an excitation wavelength of 405 nm for all other binary mixtures in the presence of GO are provided in Fig. S2 (ESI†). On gradual addition of ACN in the NaFlu GO system, it is evident that there is enhancement of fluorescence intensity, *i.e.* GO, which was responsible for quenching the fluorescence of NaFlu, now on addition of ACN to the medium promotes increment of fluorescence intensity of NaFlu. We have added ACN up to a point where the fluorescence intensity reaches the saturation value. Fluorescence resonance energy transfer (FRET), formation of non-emissive supramolecular moiety, hydrogen bonding and pi–pi interaction between the different oxygen related functional groups on GO surface are responsible for fluorescence quenching. Now on gradual addition of ACN since the enhancement of intensity occurs, we propose that ACN acts as an enhancer of fluorescence by diminishing the factors to some extent responsible for fluorescence quenching. For the final addition of ACN (χ_{ACN} = 0.062), to the NaFlu–GO mixture in water, the ABQY value of NaFlu increases to 0.42 when compared to the ABQY value of the NaFlu–GO mixture in water which is 0.34. In the absence of GO, on gradual addition of ACN, it is seen that there is no change in the absorption peak position except that the absorption intensity gradually decreases and ACN, instead of promoting fluorescence intensity, acts as a quencher, and the emission maxima remain the same (514 nm) as shown in Fig. S3 (ESI†). In the absence of GO, for the final addition of ACN (χ_{ACN} = 0.062), to NaFlu in water, the ABQY value decreases to 0.63 when compared to the ABQY value of NaFlu in neat water which is 0.92.

(b) Water–DMF. In the case of DMF, there are basically three stages of hydrogen bonding in a water–DMF binary mixture. When the volume fraction (V) of DMF, *i.e.* V_{DMF}, is less than 0.4, addition of DMF to water strengthens the hydrogen bonding network in water. However, when V_{DMF} = 0.4, the tetrahedral structure of water is destroyed, and DMF and water molecules form complexes which are DMF·3H_2O and DMF·2H_2O. Finally, when V_{DMF} reaches 0.8, the DMF–water complex is converted to the DMF·H_2O structure due to the instability of the DMF·*n*H_2O complex.[64]

In the presence of GO as shown in Fig. 5, when DMF is added the photophysical change that NaFlu undergoes is very astounding. Initially for a low DMF concentration (χ_{DMF} = 0.003), there is no such change except that the absorption intensity value increases but on gradual addition, it is observed that not only the absorption intensity value increases but the peaks at 475 nm and 452 nm experience a bathochromic shift by 12 nm and 8 nm. In short, we can infer that there is a

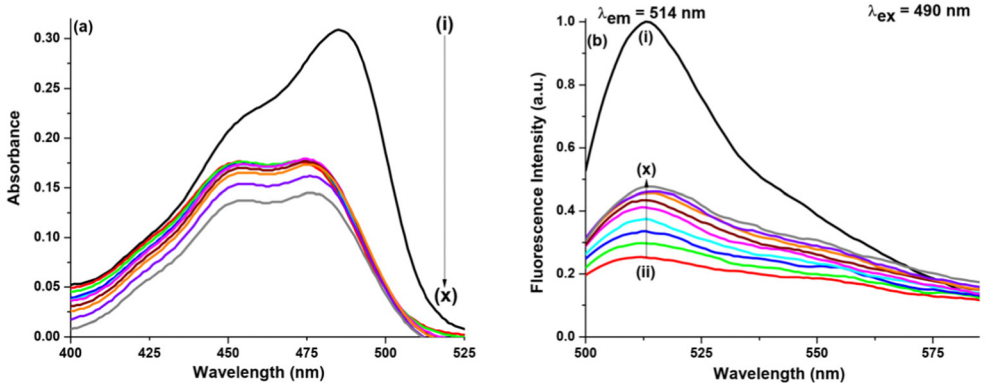

Fig. 4 (a) Absorption spectral profile and (b) fluorescence emission spectra (λ_{ex} = 490 nm) of NaFlu in the presence of GO in a water–ACN mixture: (i) NaFlu, (ii) NaFlu + 35 mg mL^{-1} GO, (iii) NaFlu + 35 mg mL^{-1} GO + ACN [χ = 0.004], (iv) NaFlu + 35 mg mL^{-1} GO + ACN [χ = 0.007], (v) NaFlu + 35 mg mL^{-1} GO + ACN [χ = 0.013], (vi) NaFlu + 35 mg mL^{-1} GO + ACN [χ = 0.018], (vii) NaFlu + 35 mg mL^{-1} GO + ACN [χ = 0.024], (viii) NaFlu + 35 mg mL^{-1} GO + ACN [χ = 0.034], (ix) NaFlu + 35 mg mL^{-1} GO + ACN [χ = 0.046], and (x) NaFlu + 35 mg mL^{-1} GO + ACN [χ = 0.062]. χ = mole fraction of ACN in the mixture.

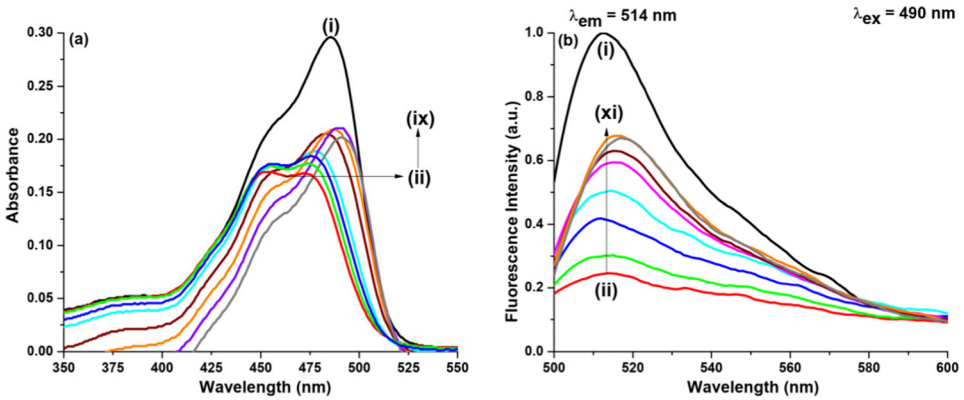

Fig. 5 (a) Absorption spectral profile and (b) fluorescence emission spectra (λ_{ex} = 490 nm) of NaFlu in the presence of GO in a water–DMF mixture: (i) NaFlu, (ii) NaFlu + 35 mg mL^{-1} GO, (iii) NaFlu + 35 mg mL^{-1} GO + DMF [χ = 0.003], (iv) NaFlu + 35 mg mL^{-1} GO + DMF [χ = 0.009], (v) NaFlu + 35 mg mL^{-1} GO + DMF [χ = 0.015], (vi) NaFlu + 35 mg mL^{-1} GO + DMF [χ = 0.035], (vii) NaFlu + 35 mg mL^{-1} GO + DMF [χ = 0.050], (viii) NaFlu + 35 mg mL^{-1} GO + DMF [χ = 0.065] and (ix) NaFlu + 35 mg mL^{-1} GO + DMF [χ = 0.080]. χ = mole fraction of DMF in the mixture.

distinguishable conversion of the monoanionic form to the dianionic form of NaFlu in the presence of GO in a water medium. When excited at 490 nm, on addition of DMF, the fluorescence intensity of NaFlu, which was quenched on addition of GO, is now drastically enhanced on addition of DMF (χ_{DMF} = 0.080) since at this point the intensity reaches the saturation value with no change in the emission position (514 nm). The corresponding spectra at the excitation wavelength are provided in the ESI.† In fact, DMF is a better enhancer than the rest of the solvents used in our study, which will be discussed later. For the addition of DMF (χ_{DMF} = 0.080), to the NaFlu–GO mixture in water, the ABQY value of NaFlu increases to 0.70. In the absence of GO, however, the trend observed in the case of DMF is almost the same, just like ACN. On addition of DMF (χ_{DMF} = 0.080), there is no considerable shift in the peak position, which is accompanied by a decrease in the absorption intensity, and DMF promotes quenching of the fluorescence intensity with the emission position appearing at 516 nm as shown in Fig. S3 (ESI†). In the absence of GO, for the addition of DMF (χ_{DMF} = 0.080), to NaFlu in water, the ABQY value decreases to 0.60 compared to the ABQY value of NaFlu in neat water (0.92).

(c) Water–DMSO. In the case of water–DMSO binary solvents it is well known that one DMSO molecule associates itself with two water molecules *via* hydrogen bonding, and hydrogen bonding between DMSO and water is more stable than hydrogen bonding between water molecules themselves. When χ_{DMSO} is 0.21 and 0.35, the water structure is unaffected by DMSO but at χ_{DMSO} = 0.35, not only DMSO-2H_2O complexes are formed but also a deviation from ideal mixing occurs, and DMSO forms complexes with two or three water molecules. Deviation of physical properties occurs when the mole fraction of DMSO is between 0.30 and 0.40. The presence of "micromicelle" arrangements in a water–DMSO mixture when χ_{DMSO} = 0.10–0.20, which accounts for the anomalous behaviour of water–DMSO binary mixtures, is also shown. Hence based on the literature, it is evident that the water–DMSO mixture exhibits anomalous behaviour when χ_{DMSO} = 0.10–

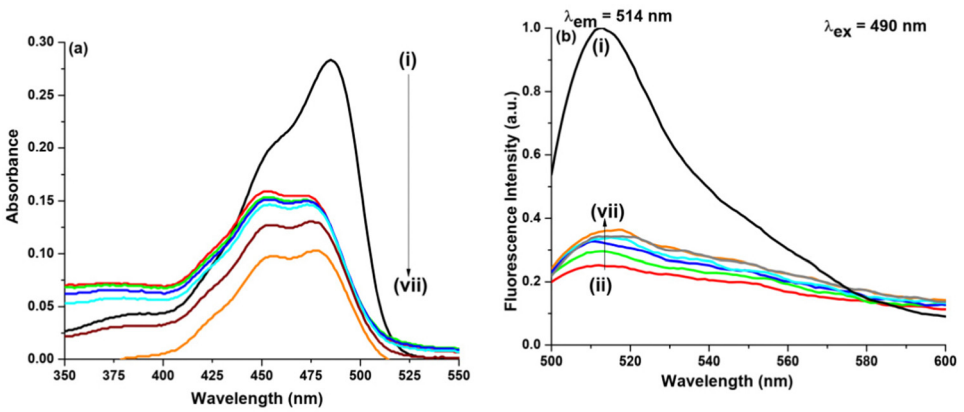

Fig. 6 (a) Absorption spectral profile and (b) fluorescence emission spectra (λ_{ex} = 490 nm) of NaFlu in the presence of GO in the water–DMSO mixture: (i) NaFlu, (ii) NaFlu + 35 mg mL^{-1} GO, (iii) NaFlu + 35 mg mL^{-1} GO + DMSO [χ = 0.004], (iv) NaFlu + 35 mg mL^{-1} GO + DMSO [χ = 0.010], (v) NaFlu + 35 mg mL^{-1} GO + DMSO [χ = 0.015], (vi) NaFlu + 35 mg mL^{-1} GO + DMSO [χ = 0.037] and (vii) NaFlu + 35 mg mL^{-1} GO + DMSO [χ = 0.060]. χ = mole fraction of DMSO in the mixture.

0.20 and 0.30–0.40. In our case, $\chi_{DMSO} < 0.10$ and thus there is no anomalous behaviour of water–DMSO binary mixtures in our study.[27]

In the presence of GO as shown in Fig. 6, on addition of DMSO ($\chi_{DMSO} = 0.004$), no such change either in the absorption peak position or the absorption intensity was observed. On gradual addition until the final addition of DMSO, the intensity amplitude of the 452 nm peak slightly decreases, whereas the intensity amplitude of the 475 nm peak slightly increases accompanied by a decrease in the absorption intensity. Here too we can say DMSO interacts with NaFlu molecules in the presence of GO. In the case of emission spectra, we have used two excitation wavelengths which are 490 nm and 405 nm. The corresponding spectra using an excitation wavelength of 405 nm for all other binary mixtures are provided in the ESI.† On gradual addition of DMSO to the NaFlu–GO system, it is evident that there is an increment in the fluorescence intensity, *i.e.* GO, which quenched the fluorescence intensity of NaFlu, now on adding DMSO to the medium enhances the fluorescence intensity. We have added DMSO ($\chi_{DMSO} = 0.060$) since at this point the fluorescence intensity saturates. Since on gradual addition of DMSO, the intensity enhances, we propose that DMSO acts as an enhancer of fluorescence with the emission peak being intact at 514 nm. For the addition of DMSO ($\chi_{DMSO} = 0.060$), to the NaFlu–GO mixture in water, the ABQY value of NaFlu increases to 0.44. Now in the absence of GO, on final addition of DMSO, it is seen that there is no such change in the absorption peak position except that the absorption intensity decreases and DMSO acts as a quencher as shown in Fig. S3 (ESI†). In the absence of GO, for the addition of DMSO ($\chi_{DMSO} = 0.060$), to NaFlu in water, the ABQY value decreases to 0.74 compared to the ABQY value of NaFlu in neat water (0.92).

(e) Water–THF. At room temperature, THF is miscible with water at any composition.[65] X-Ray scattering data reveal that the total number of water–THF and water–water bonds decreases with increasing the χ_{THF}.[65] However, the water–THF bonds are indistinguishable from the water–water hydrogen bonds. In water–THF mixtures microheterogeneity occurs when χ_{THF} is in between 0.10 and 0.50.[65] Also at low THF concentrations, the hydrogen bond of the water–water network is little affected by the hydrogen bonds formed between water and THF molecules.[66] Since in our work the χ_{THF} value is less than 0.10, there is no possibility of microheterogeneity in the water–THF binary mixtures in our study.

On addition of THF as shown in Fig. 7 ($\chi_{THF} = 0.002$), the peak at 452 nm experiences a blue shift by 15 nm, hence a new peak at 437 nm is formed with a decrease in the absorption intensity. This shows that on addition of THF to the NaFlu–GO system in water, a neutral form of the dye (437 nm) tends to exist. On excitation at 490 nm, the emission peak position remains the same (514 nm) but the intensity progressively decreases. For the addition of THF ($\chi_{THF} = 0.022$) to the NaFlu–GO mixture in water, the ABQY value of NaFlu decreases to 0.08. Now in the absence of GO, on addition of THF ($\chi_{THF} = 0.022$), it is seen that there is a prominent change in the absorption peak position with a decrease in the absorption intensity. The peak at 487 nm completely undergoes a blue shift by 12 nm and thus generates a shoulder maximum at 475 nm. The main absorption peak is generated at 435 nm which corresponds to the neutral form of the dye as shown in Fig. 7. In the absence of GO, for the addition of THF ($\chi_{THF} = 0.022$), to NaFlu in water, the ABQY value decreases to 0.05 when compared to the ABQY value of NaFlu in neat water (0.92). In the NaFlu–water system, THF acts as a quencher and the emission maxima remain the same (514 nm) when excited at 490 nm. The corresponding spectra using an excitation wavelength of 405 nm both in the presence and in the absence of GO are provided in Fig. S2 and S3 (ESI†) respectively.

We have plotted the absorption ratio of $\frac{A_{485\,nm}}{A_{460\,nm}}$ of NaFlu *vs.* the mole fraction of polar aprotic solvents which are ACN, DMF and DMSO as shown in Fig. 8. The plots obtained exhibit a non-linear correlation with the mole fraction of polar aprotic solvents indicating that hydrogen bond formation,

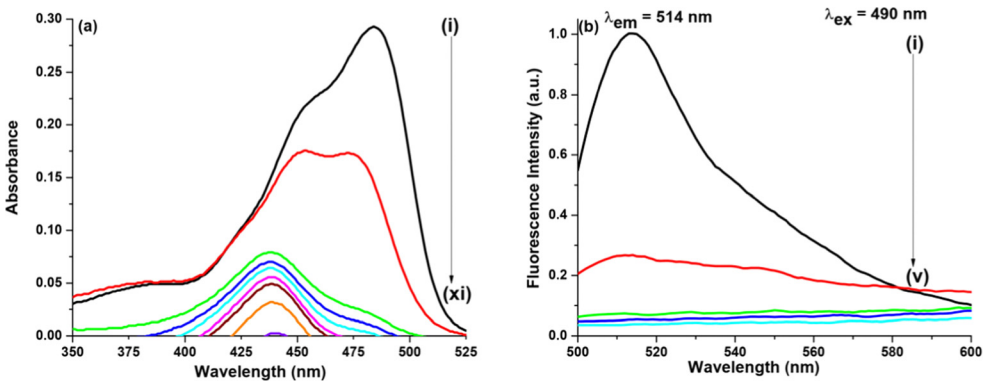

Fig. 7 (a) Absorption spectral profile of NaFlu in the presence of GO in a water–THF mixture: (i) NaFlu, (ii) NaFlu + 35 mg mL^{-1} GO, (iii) NaFlu + 35 mg mL^{-1} GO + THF [χ = 0.002], (iv) NaFlu + 35 mg mL^{-1} GO + THF [χ = 0.003], (v) NaFlu + 35 mg mL^{-1} GO + THF [χ = 0.005], (vi) NaFlu + 35 mg mL^{-1} GO + THF [χ = 0.008], (vii) NaFlu + 35 mg mL^{-1} GO + THF [χ = 0.012], (viii) NaFlu + 35 mg mL^{-1} GO + THF [χ = 0.016], and (vii) NaFlu + 35 mg mL^{-1} GO + THF [χ = 0.022]. (b) Fluorescence emission spectra (λ_{ex} = 490 nm) of NaFlu in the presence of GO in a water–THF mixture: (i) NaFlu, (ii) NaFlu + 35 mg mL^{-1} GO, (iii) NaFlu + 35 mg mL^{-1} GO + THF [χ = 0.002], (iv) NaFlu + 35 mg mL^{-1} GO + THF [χ = 0.005] and (v) NaFlu + 35 mg mL^{-1} GO + THF [χ = 0.022]. χ = mole fraction of THF in the mixture.

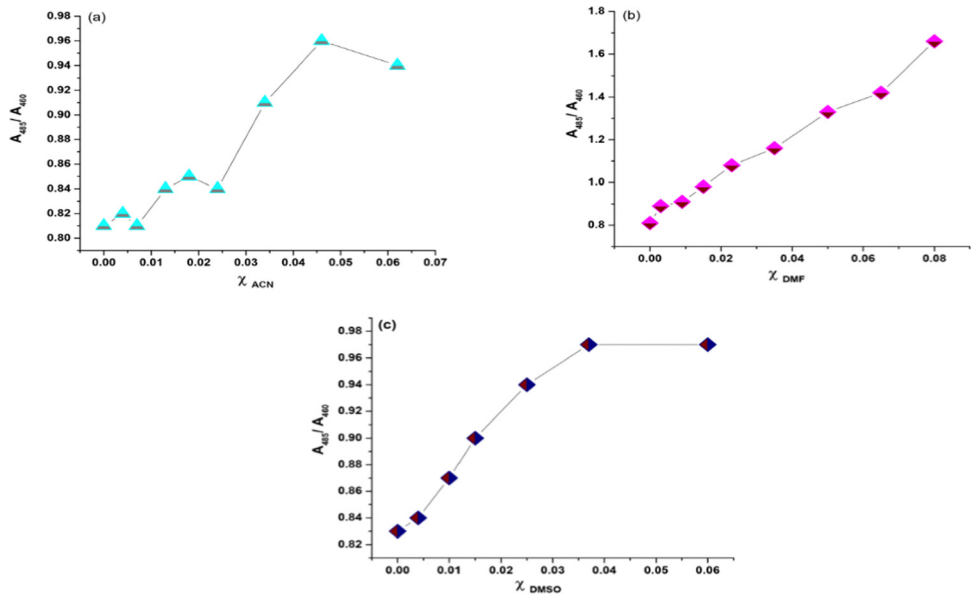

Fig. 8 The plot of absorbance ratio $\frac{A_{485\,nm}}{A_{460\,nm}}$ *vs.* mole fraction of polar aprotic solvents in the presence of GO in (a) ACN, (b) DMF and (c) DMSO.

solvation and non-ideal behaviour contribute to the obtained spectrum.[27]

3.1.5 Possible mechanism for anomalous behaviour. NaFlu is well known to exhibit aggregation-caused quenching (ACQ) properties.[61] However, it is also well documented in the literature that fluorescein and fluorescein derivatives can exhibit aggregation-induced emission (AIE).[62,67] So in the presence of GO, when ACN, DMF and DMSO are added, NaFlu molecules form aggregates. However, the emission intensity of NaFlu is enhanced. This may be due to solvent-induced aggregation which eventually leads to AIE.[62] This means that when the polar aprotic solvents are added, NaFlu forms aggregates and due to the aggregate formation there is a restriction in the intramolecular rotation of NaFlu molecules and the chances of non-radiative relaxation pathways decrease which eventually leads to the AIE phenomenon (Scheme 3). However, the AIE of NaFlu molecules follows the order water–DMF > water–ACN > water–DMSO in water–solvent binary mixtures which is observed for both 490 nm and 405 nm excitation wavelengths. In the absence of GO and in the case of THF solvent (both in the

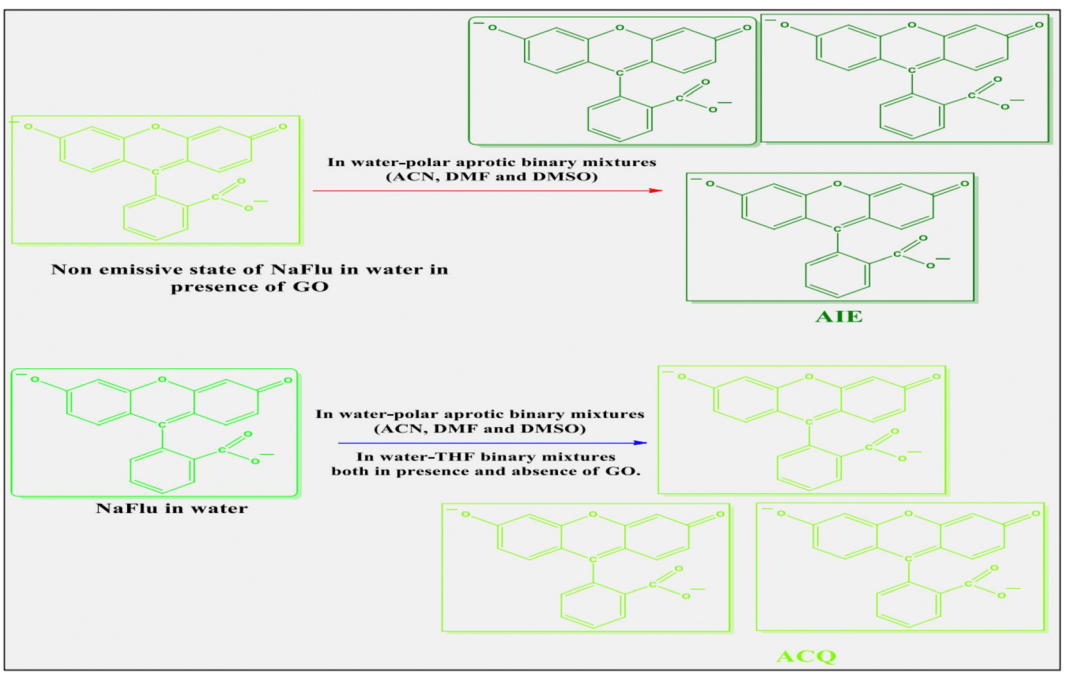

Scheme 3 ACQ and AIE of NaF in different media.

presence and in the absence of GO), ACQ is more prominent. This occurs since NaFlu forms aggregates and that aggregate formation leads to π–π coplanar interactions between NaFlu molecules, which eventually generates excimer species that prefers to decay through non-radiative pathways.[62]

3.3 Time-resolved fluorescence emission (TRFE)

3.3.1 Studies on the interaction of NaFlu with GO in water. The fluorescence emission decay of NaFlu was collected using the 405 nm excitation wavelength as shown in Fig. 9. The lifetime studies in polar aprotic solvents along with GO are available in Fig. S6 (ESI†). The lifetime value of NaFlu in neat water is 3.70 ns. This is due to the dianionic form of NaFlu. On addition of GO, *i.e.* up to 3 μg mL^{-1} GO, the lifetime value almost remains the same which is 3.72 ns. However, on further addition of 15, 35, 60 and 100 μg mL^{-1} GO, the lifetime value chronologically decreases to 3.54 ns, 3.37 ns, 3.34 ns and 3.27 ns respectively, the decay is monoexponential in nature, and it is due to the dianionic form of the dye. Thus on increasing the GO concentration dominant static quenching is prominent. Hence, NaFlu interacts with the various functional groups available on the GO surface, and the latter increases the rate of non-radiative transition. The lifetime values are tabulated in Table S2 (ESI†).

3.3.1 Studies on the interaction of NaFlu with GO in binary mixtures in the presence and in the absence of GO

(A) Water–ACN. On addition of ACN (χ_{ACN} = 0.004), the lifetime value becomes 3.42 ns as shown in Table S3 (ESI†). However, on addition of ACN (χ_{ACN} = 0.062), the lifetime value increases to 3.75 ns. All the decays exhibit a monoexponential character. From this, it is evident that ACN decreases the rate of non-radiative transition of NaFlu molecules in the NaFlu–GO system. In the absence of GO, for the addition of ACN (χ_{ACN} = 0.062), the emission decay is monoexponential in nature, and the lifetime value is 3.89 ns (Fig. 10).

(B) Water–DMF. In the presence of GO, on addition of DMF the lifetime value consistently increases, and all the decays showcase monoexponential characteristics. On addition of DMF (χ_{DMF} = 0.009), the lifetime value becomes 3.51 ns, and it is 4.02 ns for the addition of DMF (χ_{DMF} = 0.080). From this, it is evident that DMF decreases the rate of non-radiative transition in the NaFlu–GO system. In the absence of GO, for the addition of DMF (χ_{DMF} = 0.080), the decay remains monoexponential in nature and the lifetime value becomes 4.03 ns as shown in Fig. 11.

(C) Water–DMSO. In the case of DMSO and in the presence of GO, on addition of DMSO (χ_{DMSO} = 0.004), the lifetime value becomes 3.37 ns. However, on addition of DMSO (χ_{DMSO} = 0.060), the lifetime value increases to 3.66 ns. From this, it is evident that DMSO decreases the rate of non-radiative transition of NaFlu molecules in the NaFlu–GO system. In the absence of GO, for the addition of DMSO (χ_{DMSO} = 0.060), the lifetime decay remains monoexponential in nature, and the lifetime value becomes 3.85 ns (Fig. 12).

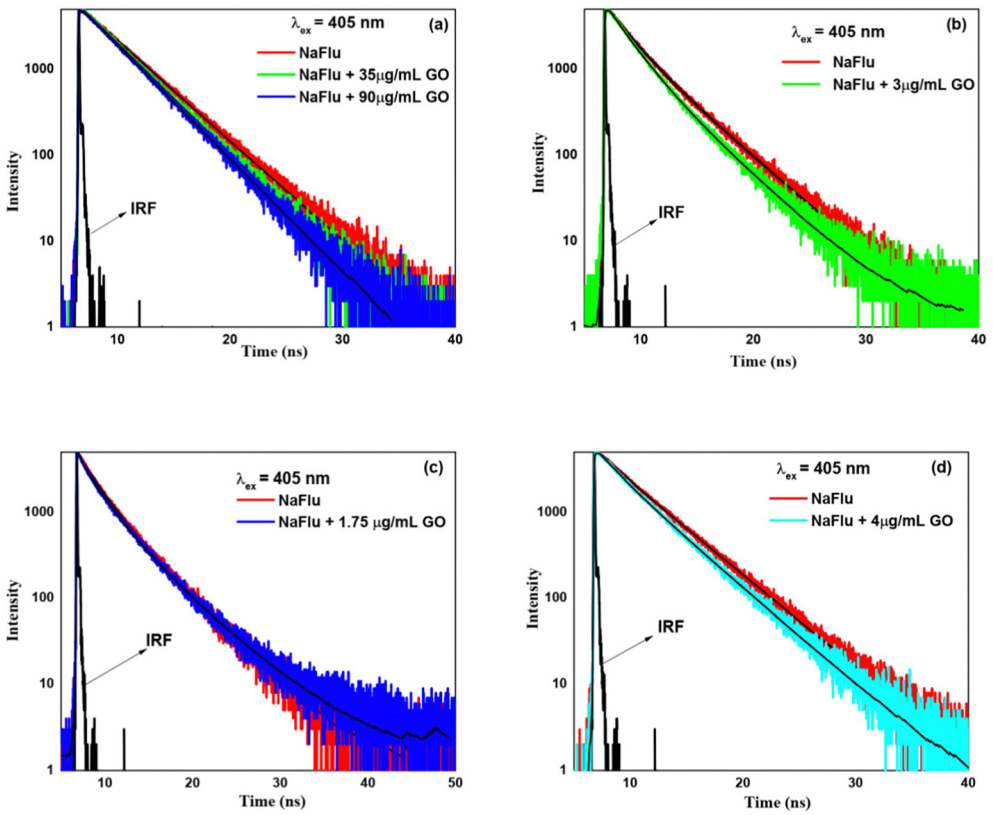

Fig. 9 Fluorescence emission decays of NaFlu with GO in (a) water, (b) ACN, (c) DMF and (d) DMSO.

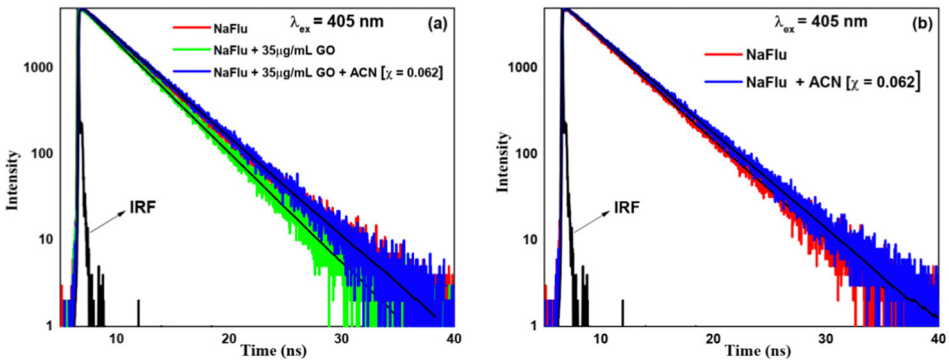

Fig. 10 Fluorescence emission decays of NaFlu in (a) a water–ACN binary mixture in the presence of GO and (b) a water–ACN binary mixture in the absence of GO.

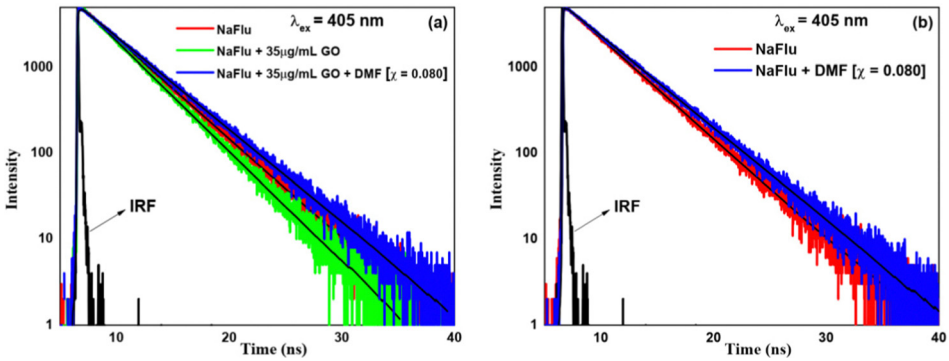

Fig. 11 Fluorescence emission decays of NaFlu in (a) a water–DMF binary mixture in the presence of GO and (b) a water–DMF binary mixture in the absence of GO.

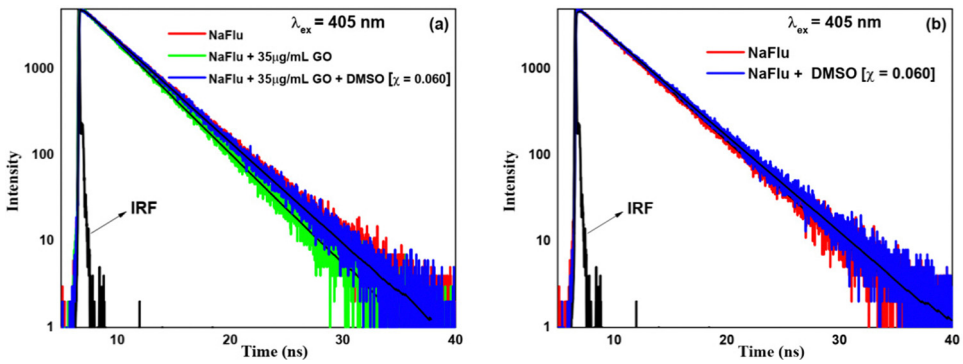

Fig. 12 Fluorescence emission decays of NaFlu in (a) a water–DMSO binary mixture in the presence of GO and (b) a water–DMSO binary mixture in the absence of GO.

(D) Water–THF. In the presence of GO, on addition of THF (χ_{THF} = 0.002), the lifetime value becomes 3.14 ns, *i.e.* no prominent change. However, on addition of THF (χ_{THF} = 0.022), the lifetime value increases and remains monoexponential in nature with a lifetime value of 3.31 ns. From this, it is evident that THF, similar to other solvents, decreases the rate of non-radiative transition of NaFlu molecules in the NaFlu–GO system. In the absence of GO, for the addition of THF (χ_{THF} = 0.022), the decay remains monoexponential in nature, and the lifetime value becomes 3.56 ns (Fig. 13).

3.4 Raman spectral study

Raman spectroscopy is a powerful, fast, and vital tool to characterize and determine the various diverse set of properties of carbon based materials such as fullerenes, diamond as well as graphite.[68] Raman spectroscopy showcases important

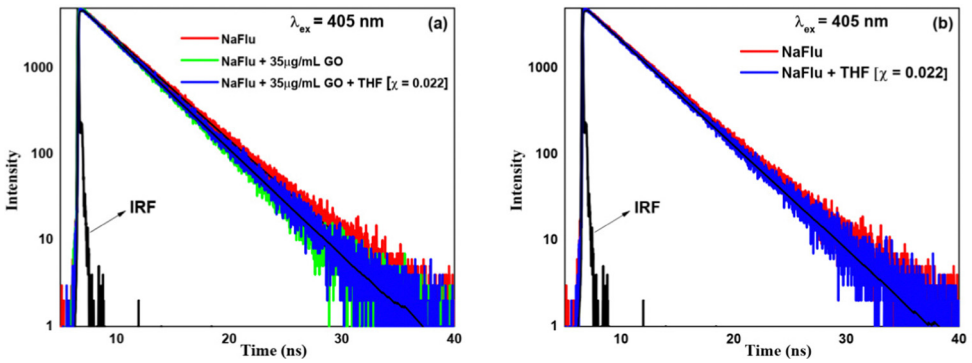

Fig. 13 Fluorescence emission decays of NaFlu in (a) a water–THF binary mixture in the presence of GO and (b) a water–THF binary mixture in the absence of GO.

features of graphene type materials.[68] Therefore, in unravelling GO's structural properties, Raman spectroscopy comes in very handy.[69] Two distinctive Raman peaks at 1586–1596 cm^{-1} and at 1336–1347 cm^{-1} are known to be formed. The presence of E_{2g} vibrational modes of carbon and sp^2 carbon atoms leads to the formation of the G band of GO which is at 1586–1596 cm^{-1}.

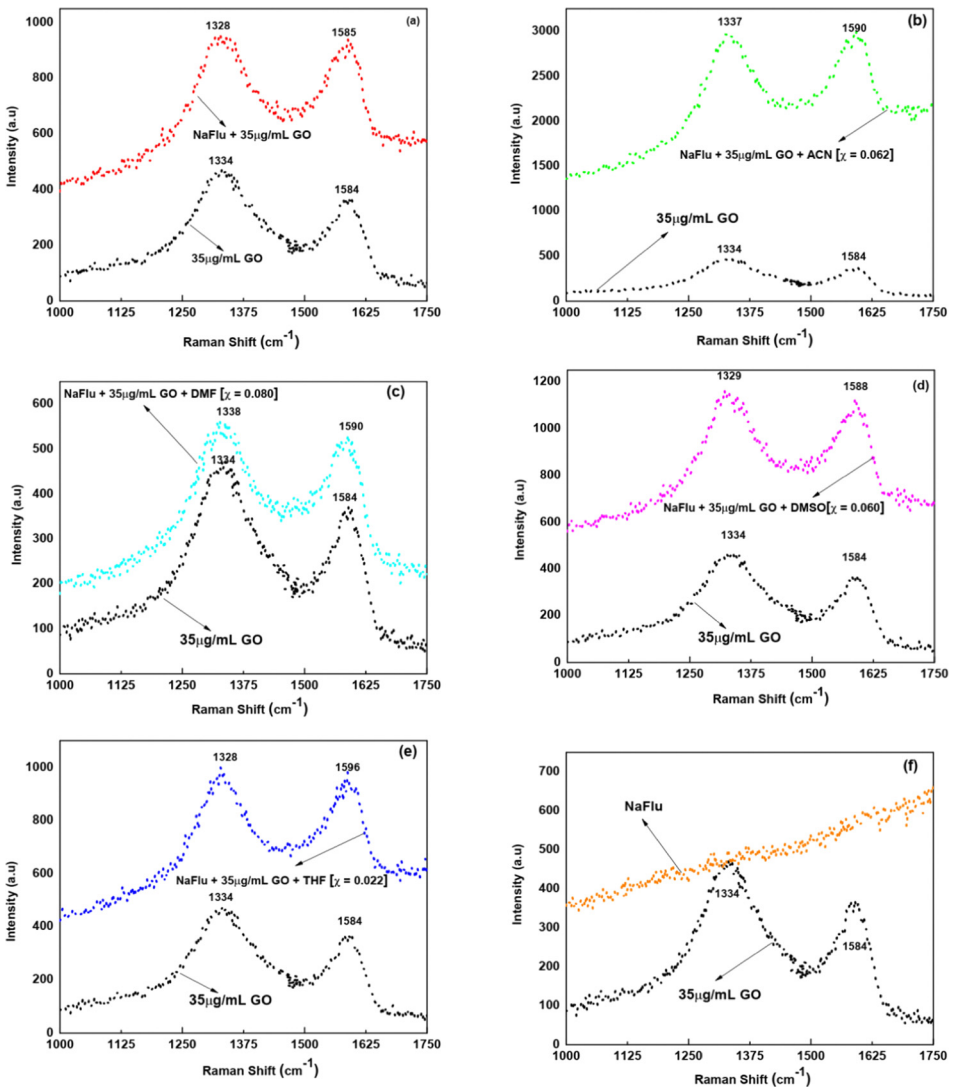

Fig. 14 Raman spectra of GO in the presence of NaFlu: (a) water, (b) water–ACN binary mixture, (c) water–DMF binary mixture, (d) water–DMSO binary mixture, and (e) water–THF binary mixture and (f) Raman spectra of NaFlu in the absence of GO.

The disordered sp^3 carbon atoms present in GO generate the D band which is at 1336–1347 cm^{-1}.[34] The parameter to comprehend the defects in bonding, the sp^3/sp^2 fraction of carbon and disordered carbon content, in graphene oxide is the $I_{(D)}/I_{(G)}$ ratio.[70,71] Several studies present in the literature demonstrate that there is a decrease[72,73] and an increase[74,75] in the $I_{(D)}/I_{(G)}$ ratio. In our work as shown in Fig. 14 we were interested to examine whether there is any surface modification of GO in the presence of binary mixtures both in the presence and in the absence of NaFlu. The $I_{(D)}/I_{(G)}$ ratio of GO for all systems is in between 1.00 and 1.20. Thus, even though there is no prominent change in the $I_{(D)}/I_{(G)}$ ratio, the distinctive peaks of GO, which are the D band and the G band, undergo a shift to both longer and shorter wavelengths followed by an enhancement in the Raman intensity. Thus even though GO does not undergo any drastic modification in its surface morphology, the change in Raman intensity along with shifts in the peak position explains the interaction of GO with the involved species *via* H-bonding, non-covalent interaction or π–π stacking. Also there are no Raman spectra of NaFlu in the region where GO exhibits

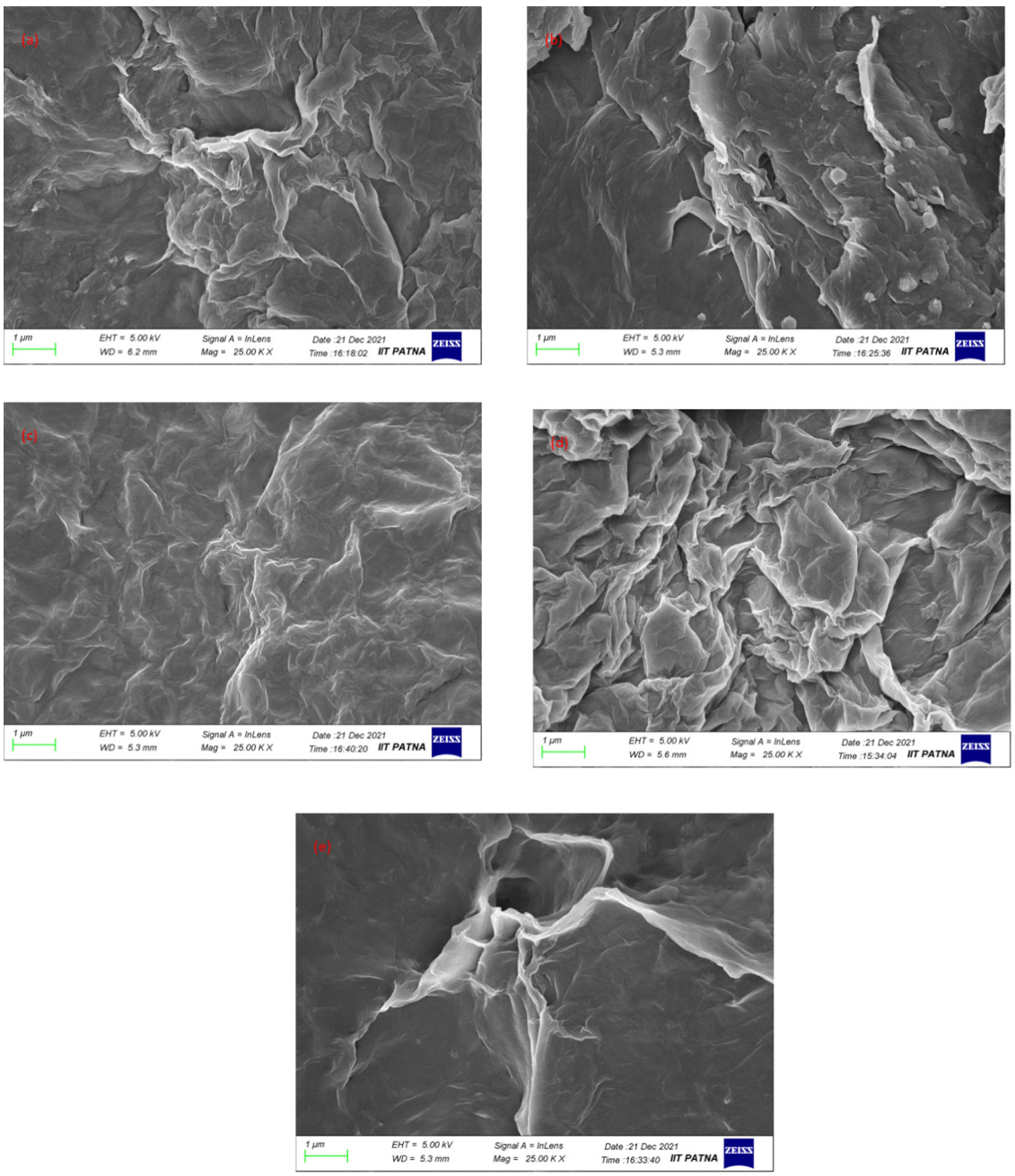

Fig. 15 FE-SEM images of GO in the presence of NaFlu (a) in neat water, (b) in a water–ACN (χ_{ACN} = 0.062) binary mixture, (c) in a water–DMF (χ_{DMF} = 0.080) binary mixture, (d) in a water–DMSO (χ_{DMSO} = 0.060) binary mixture and (e) in a water–THF (χ_{THF} = 0.022) binary mixture. χ is the mole fraction of the co-solvent.

Raman peaks as seen in Fig. 14. In the absence of NaFlu the Raman spectra are shown in Fig. S7 (ESI†).

3.5 Field emission scanning electron microscopy (FE-SEM) images of GO in different solvent mixtures

The field emission scanning electron microscopy (FE-SEM) images of GO in the presence and in the absence of NaFlu in water as well as in water–binary mixtures were obtained. The samples were first prepared and then dropped on carbon tape, dried and left overnight. Then the prepared samples were coated with gold using the ion-sputtering technique.

For comprehending the surface morphology of GO in different environments, FE-SEM is an important technique. FE-SEM images of GO in different solvents in the absence as well as in the presence of NaFlu in different media are shown in Fig. S8 (ESI†) and Fig. 15 respectively. The images of GO in different media are almost the same, which explains there is no change in the GO surface morphology. We observe that in the presence as well as in the absence of NaFlu, the surface morphology of GO in different solvent mixtures undergoes no such appreciable change. In brief FE-SEM data illustrate no structural modifications GO undergoes both in the presence and in the absence of NaFlu in different solvent mixtures.

3.6 Fluorescence lifetime imaging microscopy (FLIM)

FLIM is a unique tool to comprehend the lifetime distribution of NaFlu with GO in the solid dried state. FLIM images were obtained using a DCS-120 laser scanning confocal microscope system of Becker and Hickl (GmbH) which is equipped with an inverted optical microscope of Zeiss, controlled by a galvo-drive unit (Becker and Hickl GDA-120). DCS-120 which is equipped with a polarizing beam splitter and a hybrid GaAsP photodetector was the detector. For all the systems, we have used a 40× objective (NA: 0.75) in the microscope. The IRF of the system is less than 100 ps. The FLIM study was performed to understand the lifetime distribution of NaFlu in the presence of GO in different solvent mixtures. FLIM images (Fig. S9, ESI†) of NaFlu in the presence of GO in solvent mixtures and their corresponding intensity images are shown in Fig. S9 (ESI†) and the lifetime data are shown in Table S4 (ESI†). From the obtained images and lifetime value data, it is clear that the NaFlu molecules are adsorbed on the GO surface, and the fluorescence lifetime data of NaFlu suggest that there is homogeneous distribution of NaFlu in GO in different solvent mixtures.

4. Conclusions

In a nutshell, we have monitored the photophysical behavior of NaFlu molecules in the presence as well as in the absence of GO, in neat solvents and water–polar aprotic solvent binary mixtures. In water, on gradual addition of GO, the fluorescence intensity value of NaFlu decreases since GO acts as a quencher. However, on addition of ACN, DMF and DMSO to the NaFlu–GO system in water, the emission intensity increases. This is because polar aprotic solvents promote solvent induced aggregation of NaFlu in water, and thus AIE is very prominent since due to the aggregate formation there is a restriction in the intramolecular rotation of NaFlu molecules, and the chances of non-radiative relaxation pathways decrease which eventually leads to the AIE phenomenon. However, in the absence of GO and in the water–THF system (presence/absence of GO) NaFlu forms aggregates which leads to π–π coplanar interactions between NaFlu molecules leading to excimer formation that prefers to decay through nonradioactive pathways thus promoting the ACQ phenomenon. NaFlu molecules undergo dominant static quenching in the presence of GO with positive deviation from usual linear curvature. The adsorption of NaFlu in GO in water, ACN and DMSO is also reported in our work. The excitation spectra data also resonate with the steady state absorption data, *i.e.* justifies the form conversion of NaFlu molecules and the existence of different emissive states in the medium. To support the AIE and ACQ characteristics of NaFlu in different binary mixtures the ABQY value of NaFlu was determined in water as well as in binary mixtures both in the presence and in the absence of GO. In the presence of GO, the ABQY value of NaFlu increases when compared to that of the NaFlu–GO system in water, after addition of ACN, DMF, or DMSO to the mixture, showing aggregation-induced emission (AIE) characteristics. In the absence of GO, the ABQY value of NaFlu was decreased when compared to NaFlu in water, after addition of ACN, DMF, DMSO and THF to NaFlu in water, showing aggregation-caused quenching (ACQ) characteristics. The TRFE data also show that the rate of non-radiative transition decreases and thus the lifetime value of NaFlu in water–binary solvent mixtures increases. The Raman spectra, FESEM data and FLIM data also show that there is no change in the surface morphology of GO in water–binary solvent mixtures. In this work, NaFlu exhibits dual nature, *i.e.* ACQ and AIE in binary solvent mixtures. ACQ is observable in the absence of GO and AIE is observed in the presence of GO.

Conflicts of interest

The authors declare no conflicts of interest.

Acknowledgements

All the authors are thankful to the Indian Institute of Technology Patna, India for the research facilities. S. P. and S. B. are thankful to the Indian Institute of Technology Patna for the research fellowship.

References

1 P. D. McQueen, S. Sagoo, H. Yao and R. A. Jockusch, On the intrinsic photophysics of fluorescein, *Angew. Chem., Int. Ed.*, 2010, **49**, 9193–9196.
2 F. Naderi and A. Farajtabar, Solvatochromism of fluorescein in aqueous aprotic solvents, *J. Mol. Liq.*, 2016, **221**, 102–107.

3 A. M. Brouwer, Standards for photoluminescence quantum yield measurements in solution (IUPAC Technical Report), *Pure Appl. Chem.*, 2011, **83**, 2213–2228.
4 D. M. Al-Aqmar, H. I. Abdelkader and M. T. Abou Kana, Spectroscopic properties and amplified spontaneous emission of fluorescein laser dye in ionic liquids as green media, *Opt. Mater.*, 2015, **47**, 573–581.
5 J. Y. Jin, H. G. Kim, C. H. Hong, E. K. Suh and Y. S. Lee, White light emission from a blue LED, combined with a sodium salt of fluorescein dye, *Synth. Met.*, 2007, **157**, 138–141.
6 M. M. Abutalib, M. Shkir, I. S. Yahia, S. AlFaify, A. M. El-Naggar and V. Ganesh, Thickness dependent optical dispersion and nonlinear optical properties of nanocrystalline fluorescein dye thin films for optoelectronic applications, *Optik*, 2016, **127**, 6601–6609.
7 K. Sasazawa, Y. Yamada, A. Fujisawa, T. Saitoh, K. Ueno, K. Oharu and H. Sawada, Preparation of self-assembled fluorinated molecular aggregates, fluorescein nanocomposites: an extremely enhanced light absorption in nanocomposites, *Colloid Polym. Sci.*, 2005, **283**, 812–816.
8 M. C. Rosu, R. C. Suciu, M. D. Lazar and I. Bratu, The influence of alizarin and fluorescein on the photoactivity of Ni, Pt and Ru-doped TiO2 layers, *Mater. Sci. Eng., B*, 2013, **178**, 383–390.
9 W. A. Farooq, A. Fatehmulla, F. Yakuphanoglu, I. S. Yahia, S. M. Ali, M. Atif, M. Aslam and W. Tawfik, Photovoltaic characteristics of solar cells based on nanostructured titanium dioxide sensitized with fluorescein sodium salt, *Theor. Exp. Chem.*, 2014, **50**, 121–126.
10 R. Sasai and M. Morita, Luminous relative humidity sensing by anionic fluorescein dyes incorporated into layered double hydroxide/1-butanesulfonate hybrid materials, *Sens. Actuators, B*, 2017, **238**, 702–705.
11 H. Wang, G. Zhou, C. Mao and X. Chen, A fluorescent sensor bearing nitroolefin moiety for the detection of thiols and its biological imaging, *Dyes Pigm.*, 2013, **96**, 232–236.
12 V. Patil, V. Padalkar and N. Sekar, Environment-sensitive benzoxazole based fluorescein derivatives: Synthesis and application to the design of ON–OFF fluorescent chemosensors for microenvironment, *J. Lumin.*, 2015, **158**, 243–251.
13 J. Murube, Fluorescein: Its use in investigation of lacrimal characteristics, *Ocul. Surf.*, 2013, **4**, 212–218.
14 K. S. Novoselov, A. K. Geim, S. V. Morozov, D. E. Jiang, Y. Zhang, S. V. Dubonos, I. V. Grigorieva and A. A. Firsov, Electric field effect in atomically thin carbon films, *Science*, 2004, **306**, 666–669.
15 V. C. Sanchez, A. Jachak, R. H. Hurt and A. B. Kane, Biological interactions of graphene-family nanomaterials: an interdisciplinary review, *Chem. Res. Toxicol.*, 2012, **25**, 15–34.
16 C. Bussy, H. Ali-Boucetta and K. Kostarelos, Safety considerations for graphene: lessons learnt from carbon nanotubes, *Acc. Chem. Res.*, 2013, **46**, 692–701.
17 P. Zhu, B. G. Sumpter and V. Meunier, Electronic, thermal, and structural properties of graphene oxide frameworks, *J. Phys. Chem. C*, 2013, **117**, 8276–8281.
18 A. A. Balandin, Thermal properties of graphene and nanostructured carbon materials, *Nat. Mater.*, 2011, **10**, 569–581.
19 S. Stankovich, D. A. Dikin, R. D. Piner, K. A. Kohlhaas, A. Kleinhammes, Y. Jia, Y. Wu, S. T. Nguyen and R. S. Ruoff, Synthesis of graphene-based nanosheets *via* chemical reduction of exfoliated graphite oxide, *Carbon*, 2007, **45**, 1558–1565.
20 G. Zhao, J. Li, X. Ren, C. Chen and X. Wang, Few-layered graphene oxide nanosheets as superior sorbents for heavy metal ion pollution management, *Environ. Sci. Technol.*, 2011, **45**, 10454–10462.
21 C. Chung, Y. K. Kim, D. Shin, S. R. Ryoo, B. H. Hong and D. H. Min, Biomedical applications of graphene and graphene oxide, *Acc. Chem. Res.*, 2013, **46**, 2211–2224.
22 V. Georgakilas, J. N. Tiwari, K. C. Kemp, J. A. Perman, A. B. Bourlinos, K. S. Kim and R. Zboril, Noncovalent functionalization of graphene and graphene oxide for energy materials, biosensing, catalytic, and biomedical applications, *Chem. Rev.*, 2016, **116**, 5464–5519.
23 Y. Yin, K. Hu, A. M. Grant, Y. Zhang and V. V. Tsukruk, Biopolymeric nanocomposites with enhanced interphases, *Langmuir*, 2015, **31**, 10859–10870.
24 J. Zhang, L. Chen, B. Shen, L. Chen, J. Mo and J. Feng, Dual-sensitive graphene oxide loaded with proapoptotic peptides and anticancer drugs for cancer synergetic therapy, *Langmuir*, 2019, **35**, 6120–6128.
25 H. Kim, R. Namgung, K. Singha, I. K. Oh and W. J. Kim, Graphene oxide–polyethylenimine nanoconstruct as a gene delivery vector and bioimaging tool, *Bioconjugate Chem.*, 2011, **22**, 2558–2567.
26 C. H. Lu, C. L. Zhu, J. Li, J. J. Liu, X. Chen and H. H. Yang, Using graphene to protect DNA from cleavage during cellular delivery, *Chem. Commun.*, 2010, **46**, 3116–3118.
27 R. Sahoo, R. Jana and D. Seth, Photophysics of harmaline in solvent mixtures, *J. Mol. Liq.*, 2019, **275**, 84–90.
28 S. Roy, S. Banerjee, N. Biyani, B. Jana and B. Bagchi, Theoretical and computational analysis of static and dynamic anomalies in water– DMSO binary mixture at low DMSO concentrations. *The*, *J. Phys. Chem. B*, 2011, **115**, 685–692.
29 J. B. Mills, C. T. Mant and R. S. Hodges, One-step purification of a recombinant protein from a whole cell extract by reversed-phase high-performance liquid chromatography, *J. Chromatogr. A*, 2006, **1133**, 248–253.
30 U. D. Neue, *HPLC columns. Theory, Technology, and Practice*, 1997.
31 T. Welton and C. Reichardt, *Solvents and solvent effects in organic chemistry*, John Wiley & Sons, 2011.
32 S. S. N. Murthy, Some insight into the physical basis of the cryoprotective action of dimethyl sulfoxide and ethylene glycol, *Cryobiology*, 1998, **36**, 84–96.
33 U. Taşdemir, S. Büyükleblebici, P. B. Tuncer, E. Coşkun, T. Özgürtaş, F. N. Aydın, O. Büyükleblebici and İ. S. Gürcan, Effects of various cryoprotectants on bull sperm quality, DNA integrity and oxidative stress parameters, *Cryobiology*, 2013, **66**, 38–42.

34 A. Bapli, R. K. Gautam, S. Seth, R. Jana, S. Pandit and D. Seth, Graphene oxide as an enhancer of fluorescence, *Chem. – Asian J.*, 2020, **15**, 1296–1300.
35 A. Bapli, R. Jana, S. Pandit and D. Seth, Selective prototropism of lumichrome in the liposome/graphene oxide interface: A detailed spectroscopic study, *J. Mol. Liq.*, 2021, **339**, 116738.
36 A. Bapli, S. Seth, S. Pandit and D. Seth, Graphene oxide-controlled neutral versus cationic form of a red emitting dye: enhancement of fluorescence by graphene oxide, *Chem. Commun.*, 2021, **57**, 11855–11858.
37 S. Pandit, S. Seth, A. Bapli, S. Bhattacharjee and D. Seth, Graphene Oxide Induced Prototropism in Different Solvents: Enhancement of Fluorescence Induced by Graphene Oxide, *J. Mol. Liq.*, 2023, 120880.
38 F. Naderi, A. Farajtabar and F. Gharib, Solvatochromic and preferential solvation of fluorescein in some water–alcoholic mixed solvents, *J. Mol. Liq.*, 2014, **190**, 126–132.
39 A. C. Morosanu, D. G. Dimitriu and D. O. Dorohoi, Excited state dipole moment of the fluorescein molecule estimated from electronic absorption spectra, *J. Mol. Struct.*, 2019, **1180**, 723–732.
40 S. De and R. Kundu, Spectroscopic studies with fluorescein dye—Protonation, aggregation and interaction with nanoparticles, *J. Photochem. Photobiol., A*, 2011, **223**, 71–81.
41 R. Sjöback, J. Nygren and M. Kubista, Absorption and fluorescence properties of fluorescein, *Spectrochim. Acta, Part A*, 1995, **51**, L7–L21.
42 M. Anju, A. K. Akhila and N. K. Renuka, Non-covalently functionalised rGO–fluorescein unit for selective detection of fluoride ions, *Nano-Struct. Nano-Objects*, 2020, **24**, 100606.
43 C. J. Shih, S. Lin, R. Sharma, M. S. Strano and D. Blankschtein, Understanding the pH-dependent behavior of graphene oxide aqueous solutions: a comparative experimental and molecular dynamics simulation study, *Langmuir*, 2012, **28**, 235–241.
44 J. Kim, L. J. Cote, F. Kim, W. Yuan, K. R. Shull and J. Huang, Graphene oxide sheets at interfaces, *J. Am. Chem. Soc.*, 2010, **132**, 8180–8186.
45 Z. Liu, J. T. Robinson, X. Sun and H. Dai, PEGylated nanographene oxide for delivery of water-insoluble cancer drugs, *J. Am. Chem. Soc.*, 2008, **130**, 10876–10877.
46 J. S. Park, H. K. Na, D. H. Min and D. E. Kim, Desorption of single-stranded nucleic acids from graphene oxide by disruption of hydrogen bonding, *Analyst*, 2013, **138**, 1745–1749.
47 J. Kim, S. J. Park and D. H. Min, Emerging approaches for graphene oxide biosensor, *Anal. Chem.*, 2017, **89**, 232–248.
48 P. Mandal, M. Bardhan and T. Ganguly, A detailed spectroscopic study on the interaction of Rhodamine 6G with human hemoglobin, *J. Photochem. Photobiol., B*, 2010, **99**, 78–86.
49 D. Li, M. B. Müller, S. Gilje, R. B. Kaner and G. G. Wallace, Processable aqueous dispersions of graphene nanosheets, *Nat. Nanotechnol.*, 2008, **3**, 101–105.
50 R. F. Delgadillo and L. J. Parkhurst, Spectroscopic properties of fluorescein and rhodamine dyes attached to DNA, *Photochem. Photobiol.*, 2010, **86**, 261–272.
51 X. F. Zhang, X. Cui, Q. Liu and F. Zhang, Multiple-Charge Separation in Nanoscale Artificial Photosynthetic Models, *Chem. Phys. Chem.*, 2008, **9**, 1514–1518.
52 X. F. Zhang, X. Cui, Q. Liu and F. Zhang, Photoinduced multi-electron transfer in the D n–A system consisting of multi-phthalocyanines linked to one carbon nanotube, *Phys. Chem. Chem. Phys.*, 2009, **11**, 3566–3572.
53 E. Ciotta, P. Prosposito and R. Pizzoferrato, Positive curvature in Stern–Volmer plot described by a generalized model for static quenching, *J. Lumin.*, 2019, **206**, 518–522.
54 D. Peak, T. C. Werner, R. M. Dennin Jr and J. K. Baird, Fluorescence quenching at high quencher concentrations, *J. Chem. Phys.*, 1983, **79**, 3328–3335.
55 J. Keizer, Nonlinear fluorescence quenching and the origin of positive curvature in Stern–Volmer plots, *J. Am. Chem. Soc.*, 1983, **105**, 1494–1498.
56 D. K. Singh, P. K. Iyer and P. K. Giri, Role of molecular interactions and structural defects in the efficient fluorescence quenching by carbon nanotubes, *Carbon*, 2012, **50**, 4495–4505.
57 J. Wang, D. Wang, E. K. Miller, D. Moses, G. C. Bazan and A. J. Heeger, Photoluminescence of water-soluble conjugated polymers: Origin of enhanced quenching by charge transfer, *Macromolecules*, 2000, **33**, 5153–5158.
58 E. Ciotta, S. Paoloni, M. Richetta, P. Prosposito, P. Tagliatesta, C. Lorecchio, I. Venditti, I. Fratoddi, S. Casciardi and R. Pizzoferrato, Sensitivity to heavy-metal ions of unfolded fullerene quantum dots, *Sensors*, 2017, **17**, 2614.
59 K. Campbell, A. Zappas, U. Bunz, Y. S. Thio and D. G. Bucknall, Fluorescence quenching of a poly (paraphenylene ethynylenes) by C60 fullerenes, *J. Photochem. Photobiol., A*, 2012, **249**, 41–46.
60 A. Paudics, S. Farah, I. Bertóti, A. Farkas, K. László, M. Mohai, G. Sáfrán, A. Szilágyi and M. Kubinyi, Fluorescence probing of binding sites on graphene oxide nanosheets with Oxazine 1 dye, *Appl. Surf. Sci.*, 2021, **541**, 148451.
61 D. Ding, K. Li, B. Liu and B. Z. Tang, Bioprobes based on AIE fluorogens, *Acc. Chem. Res.*, 2013, **46**, 2441–2453.
62 Z. He, C. Ke and B. Z. Tang, Journey of aggregation-induced emission research, *ACS Omega*, 2018, **3**, 3267–3277.
63 N. Klonis, A. H. Clayton, E. W. Voss Jr and W. H. Sawyer, Spectral properties of fluorescein in solvent–water mixtures: applications as a probe of hydrogen bonding environments in biological systems, *Photochem. Photobiol.*, 1998, **67**, 500–510.
64 B. Yang, H. Lang, Z. Liu, S. Wang, Z. Men and C. Sun, Three stages of hydrogen bonding network in DMF–water binary solution, *J. Mol. Liq.*, 2021, **324**, 114996.
65 M. Katayama and K. Ozutsumi, The number of water–water hydrogen bonds in water-tetrahydrofuran and water-acetone binary mixtures determined by means of X-ray scattering, *J. Solution Chem.*, 2008, **37**, 841–856.
66 L. C. G. Freitas and J. M. M. Cordeiro, Monte Carlo simulation of water-tetrahydrofuran mixtures, *J. Mol. Struct.: THEOCHEM*, 1995, **335**(1–3), 189–195.
67 S. Feng, S. Gong and G. Feng, Aggregation-induced emission and solid fluorescence of fluorescein derivatives, *Chem. Commun.*, 2020, **56**, 2511–2513.

68 J. B. Wu, M. L. Lin, X. Cong, H. N. Liu and P. H. Tan, Raman spectroscopy of graphene-based materials and its applications in related devices, *Chem. Soc. Rev.*, 2018, **47**, 1822–1873.
69 D. López-Díaz, M. Lopez Holgado, J. L. García-Fierro and M. M. Velázquez, Evolution of the Raman spectrum with the chemical composition of graphene oxide, *J. Phys. Chem. C*, 2017, **121**, 20489–20497.
70 A. C. Ferrari and J. Robertson, Interpretation of Raman spectra of disordered and amorphous carbon, *Phys. Rev. B: Condens. Matter Mater. Phys.*, 2000, **61**, 14095.
71 M. A. Pimenta, G. Dresselhaus, M. S. Dresselhaus, L. G. Cancado, A. Jorio and R. Saito, Studying disorder in graphite-based systems by Raman spectroscopy, *Phys. Chem. Chem. Phys.*, 2007, **9**, 1276–1290.
72 J. I. Paredes, S. Villar-Rodil, P. Solís-Fernández, A. Martínez-Alonso and J. M. D. Tascon, Atomic force and scanning tunneling microscopy imaging of graphene nanosheets derived from graphite oxide, *Langmuir*, 2009, **25**, 5957–5968.
73 Y. Zhou, Q. Bao, L. A. L. Tang, Y. Zhong and K. P. Loh, Hydrothermal dehydration for the ''green'' reduction of exfoliated graphene oxide to graphene and demonstration of tunable optical limiting properties, *Chem. Mater.*, 2009, **21**, 2950–2956.
74 S. Stankovich, D. A. Dikin, R. D. Piner, K. A. Kohlhaas, A. Kleinhammes, Y. Jia, Y. Wu, S. T. Nguyen and R. S. Ruoff, Synthesis of graphene-based nanosheets *via* chemical reduction of exfoliated graphite oxide, *Carbon*, 2007, **45**, 1558–1565.
75 Y. Xu, H. Bai, G. Lu, C. Li and G. Shi, Flexible graphene films *via* the filtration of water-soluble noncovalent functionalized graphene sheets, *J. Am. Chem. Soc.*, 2008, **130**, 5856–5857.

